ELSEVIER

A mathematical model of plants as ecosystem engineers

E. Gilad[a,b], J. von Hardenberg[c,d], A. Provenzale[c,d], M. Shachak[e], E. Meron[a,b,*]

[a]*Department of Physics, Ben-Gurion University, Beer Sheva 84105, Israel*
[b]*Department of Solar Energy and Environmental Physics, BIDR, Ben Gurion University, Sede Boker Campus 84990, Israel*
[c]*ISAC-CNR, Corso Fiume 4, I-10133 Torino, Italy*
[d]*CIMA, Università di Genova e della Basilicata, Via Cadorna 7, 17100 Savona, Italy*
[e]*Mitrani Department of Desert Ecology, BIDR, Ben Gurion University, Sede Boker Campus 84990, Israel*

Abstract

Understanding the structure and dynamics of plant communities in water-limited systems often calls for the identification of ecosystem engineers—key species that modify the landscape, redistribute resources and facilitate the growth of other species. Shrubs are excellent examples; they self-organize to form patterns of mesic patches which provide habitats for herbaceous species. In this paper we present a mathematical model for studying ecosystem engineering by woody plant species in drylands. The model captures various feedbacks between biomass and water including water uptake by plants' roots and increased water infiltration at vegetation patches. Both the uptake and the infiltration feedbacks act as mechanisms for vegetation pattern formation, but have opposite effects on the water resource; the former depletes the soil-water content under a vegetation patch, whereas the latter acts to increase it. Varying the relative strength of the two feedbacks we find a trade-off between the engineering capacity of a plant species and its resilience to disturbances. We further identify two basic soil-water distributions associated with engineering at the single patch level, hump-shaped and ring-shaped, and discuss the niches they form for herbaceous species. Finally, we study how pattern transitions at the landscape level feedback to the single patch level by affecting engineering strength.
© 2006 Elsevier Ltd. All rights reserved.

Keywords: Ecosystem engineer; Mathematical modeling; Feedback; Instability; Resilience; Vegetation patterns; Drylands

1. Introduction

Landscapes of water-limited systems are mosaics of patches that differ in resource concentration, biomass production and species richness. Two processes affecting their structure and dynamics have attracted considerable attention during the past decade, ecosystem engineering (Jones et al., 1994, 1997; Olding-Smee et al., 2003) and self-organized patchiness (Rietkerk et al., 2004). Ecosystem engineers are key species that modify the abiotic environ-ment, redistribute resources and facilitate the growth of other species. A well studied example is provided by shrubs that concentrate soil water and form fertile patches where annuals, grasses and other species can grow (Boeken and Shachak, 1994; Pugnaire and Luque, 2001). Self-organized patchiness is a pattern formation phenomenon whereby positive water-biomass feedbacks at the level of a single patch result in vegetation patterns at the landscape level. A striking example of this phenomenon is banded vegetation on hill slopes (Valentin et al., 1999).

Progress in understanding self-organized patchiness has largely been due to the development of mathematical models of vegetation growth (Lefever and Lejeune, 1997; Klausmeier, 1999; von Hardenberg et al., 2001; Okayasu and Aizawa, 2001; Rietkerk et al., 2002; Shnerb et al., 2003). The input information used in formulating these models is at the level of a single plant-patch, while the

*Corresponding author. Blaustein Institutes for Desert Research, Ben-Gurion University, Sede Boqer Campus, 84990 Midreshet Ben-Gurion, Israel. Tel.: +972 86477556; fax: +972 86472904.

E-mail addresses: gilade@bgu.ac.il (E. Gilad),
J.VonHardenberg@isac.cnr.it (J. von Hardenberg),
A.Provenzale@isac.cnr.it (A. Provenzale), shachak@bgu.ac.il
(M. Shachak), ehud@bgu.ac.il (E. Meron).

predictive power extends to the patchwork created at the landscape level. These models reproduce various biomass patterns observed in the field (Rietkerk et al., 2004), predict the possible coexistence of different stable patterns under given environmental conditions, and identify a generic sequence of basic pattern states along the rainfall gradient (von Hardenberg et al., 2001; Meron et al., 2004).

Despite the relative success in reproducing biomass patchiness, current models (Rietkerk et al., 2004) provide very limited information about the dynamics and the spatial distributions of the soil-water resource, and thus about engineering. In general, the water resource is coupled to the plant biomass through various feedback processes including reduced evaporation by shading ("shading feedback"), increased infiltration at vegetation patches ("infiltration feedback") and water uptake by plants' roots ("uptake feedback"). The first two processes act to concentrate the water resource at vegetation patches, thus acting as positive feedbacks. The water-uptake process acts to deplete the water resource, and in this sense can be regarded as a negative feedback. Current models (Okayasu and Aizawa, 2001; Rietkerk et al., 2002) take into account all three feedbacks but overlook an important ingredient of the water uptake process: root-system augmentation in response to biomass growth. This ingredient induces positive feedback relationships between biomass and water, for it acts to *increase* the amount of soil water available to the plant by probing larger soil volumes. To capture this effect, it is necessary to model explicitly the non-locality of water uptake: uptake at a given spatial point is also due to distant plants whose roots extend to that point. Root-system augmentation affects the soil-water distribution as well as the capability of plants to withstand water stress, and is therefore an essential component in modeling plants as ecosystem engineers.

In this paper we present and study a mathematical model for vegetation growth in water-limited systems that captures root-system augmentation through non-local terms in the model equations. We first use the model to study biomass patterns along aridity gradients and reproduce results obtained with earlier models. We then study ecosystem engineering, addressing aspects such as resilience to disturbances, engineering niches and the effects of spatial patterning at the landscape level. A brief account of the model to be presented here has been given in Gilad et al. (2004).

2. Background

Ecosystem dynamics at the landscape level involve a multitude of interacting species with many traits in respect to resource acquisition and distribution. Some species, however, have greater impacts than others in the sense that their introduction or removal can dramatically alter the ecosystem's behavior. One example are "keystone species" (Power et al., 1996), whose roles in energy flow and nutrient cycling can affect the trophic web structure of the system. Recently, another type of key species, named "ecosystem engineers" (Jones et al., 1994, 1997; Olding-Smee et al., 2003), has been identified. Unlike keystone species, which directly affect the biotic component, ecosystem engineers affect the physical environment, thereby changing resource distributions and, as a result, species diversity and ecosystem functioning (Odling-Smee, 1988; Jones et al., 1994, 1997; Shachak and Jones, 1995; Gurney and Lawton, 1996; Perry, 1998; Laland et al., 1999; Shachak et al., 2005).

Processes of resource distribution are normally combinations of biotic factors, associated with ecosystem engineers, and abiotic factors. One abiotic factor contributing to water redistribution in drylands is dust and sediment deposition in rocky watersheds (Yair and Shachak, 1987). The higher water infiltration rates in deposition patches induce source-sink water flow relationships and enrich the water content in these patches. Biotic factors include cyanobacteria that form partially impermeable biogenic crusts, limiting infiltration of rainfall and favoring surface runoff generation, and plants, particularly shrubs, that act as sinks for the surface-water flow. The accumulation of litter and dust under the shrub forms a mound with high infiltration capacity, which not only absorbs direct rainfall but also intercepts the runoff water generated by the soil crust. Reduced evaporation under the shrub canopy further contributes to local water accumulation. The water-enriched patch and the accumulated dust and litter create an island of fertility (Charley and West, 1975) under the shrub canopy, characterized by higher concentration of water, nutrient and organic matter as compared with the surrounding crusted soil.

At the landscape level self-organization processes generating spatial patch patterns may take place. Depending on environmental conditions (rainfall, topography, grazing stress, etc.) and species traits, different vegetation patterns have been observed, including band, labyrinth, spot, and gap patterns (Valentin et al., 1999; Rietkerk et al., 2002, 2004; Meron et al., 2004). The self-organization of vegetation in water-limited systems to form spatial patterns has been attributed to an instability (Cross and Hohenberg, 1993; Murray, 1993) of uniform vegetation which has been produced by several independent models (Lefever and Lejeune, 1997; von Hardenberg et al., 2001; Okayasu and Aizawa, 2001; Rietkerk et al., 2002; Gilad et al., 2004). The mechanism of the instability is based on positive-feedback relationships between biomass and water. One realization of such a feedback is the increased infiltration of surface water at vegetation patches discussed above. Another realization of a positive water-biomass feedback is root-system augmentation; the larger the biomass the bigger the root system and the more soil water the roots can take up. This feedback, which is crucial for understanding ecosystem engineering, is not captured by earlier mathematical models. Another aspect of vegetation patterns that escaped attention in earlier theoretical studies is how pattern dynamics at the landscape level affect water distribution at the single patch level.

3. The model

We introduce a model for a single plant species where the limiting resource is water. A "patch" in the context of the model is defined to be an area covered by the plant, which generally differs in its water content from the surrounding bare soil. The model contains three dynamical variables: (a) the biomass density variable, $B(\mathbf{X}, T)$, representing the plant's biomass above ground level in units of (kg/m^2), (b) the soil-water density variable, $W(\mathbf{X}, T)$, describing the amount of soil water available to the plants per unit area of ground surface in units of (kg/m^2), and (c) the surface water variable, $H(\mathbf{X}, T)$, describing the height of a thin water layer above ground level in units of (mm). Rainfall and topography are introduced parametrically; thus vegetation feedbacks on climate and soil erosion are assumed to be negligible. The model equations are:

$$B_T = G_B B(1 - B/K) - MB + D_B \nabla^2 B,$$
$$W_T = IH - N(1 - RB/K)W - G_W W + D_W \nabla^2 W,$$
$$H_T = P - IH + D_H \nabla^2 (H^2) + 2D_H \nabla H \cdot \nabla Z + 2D_H H \nabla^2 Z,$$

$$(1)$$

where the subscript T denotes the partial time derivative, $\mathbf{X} = (X, Y)$ and $\nabla^2 = \partial_X^2 + \partial_Y^2$. In the biomass equation the quantity G_B represents the biomass growth rate, the parameter K is the maximum standing biomass, the parameter M is the rate of biomass loss (due to mortality and various disturbances such as grazing), and the term $D_B \nabla^2 B$ represents seed dispersal. In the soil-water equation the quantity I represents the infiltration rate of surface water into the soil, the parameter N is the soil-water evaporation rate, the parameter R describes the reduction in soil-water evaporation rate due to shading, the quantity G_W represents the soil water consumption rate, and the term $D_W \nabla^2 W$ describes soil-water transport in non-saturated soil (Hillel, 1998). Finally, in the surface-water equation the parameter P is the precipitation rate, $Z(\mathbf{X})$ is a topography function describing the ground surface height for non-flat topographies, and the parameter D_H represents the phenomenological bottom friction coefficient between the surface water and the ground surface.

While the equations for B and W are purely phenomenological (resulting from modeling processes at the single patch scale), the equation for H was motivated by shallow water theory. The shallow water approximation is based on the assumption of a thin layer of water where pressure variations are very small and the motion becomes almost two-dimensional (Weiyan, 1992).

The infiltration and uptake feedback processes are modeled in the equations through the explicit forms of the infiltration rate term I and the growth and consumption rate terms G_B and G_W. The infiltration feedback is modeled by assuming a monotonously increasing dependence of I on biomass; the bigger the biomass the higher the infiltration rate and the more soil water available to the plants. This form of the infiltration feedback mirrors the fact that in many arid regions infiltration is low far from vegetation patches due to the presence of the biogenic crust. Conversely, the presence of shrubs destroys the cyanobacterial crust and favor water infiltration. The uptake feedback is modeled by assuming a monotonously increasing dependence of the root-system size on biomass; the bigger the biomass the more extended the root system and the bigger amount of soil water the roots take up from the soil.

The explicit dependence of the infiltration rate of surface water into the soil on the biomass density is chosen as (Walker et al., 1981; HilleRisLambers et al., 2001):

$$I = A \frac{B(\mathbf{X}, T) + Qf}{B(\mathbf{X}, T) + Q},$$

$$(2)$$

where A, Q and f are constant parameters. Two distinct limits of this term (illustrated in Fig. 1) are noteworthy. When $B \to 0$, this term represents the infiltration rate in bare soil, $I = Af$. When $B \gg Q$ it represents infiltration rate in fully vegetated soil, $I = A$. The parameter Q represents a reference biomass beyond which the plant approaches its full capacity to increase the infiltration rate. The difference between the infiltration rates in bare and vegetated soil (hereafter the "infiltration contrast") is quantified by the parameter f, defined to span the range $0 \leqslant f \leqslant 1$. When $f \ll 1$ the infiltration rate in bare soil is much smaller than the rate in vegetated soil. Such values can model bare soils covered by biological crusts (Campbell et al., 1989; West, 1990). As f gets closer to 1, the infiltration rate becomes independent of the biomass density B, representing non-crusted soil where the infiltration is high everywhere. Thus, the parameter f measures the strength of the positive feedback due to increased infiltration at vegetation patches. The smaller f the stronger the feedback effect.
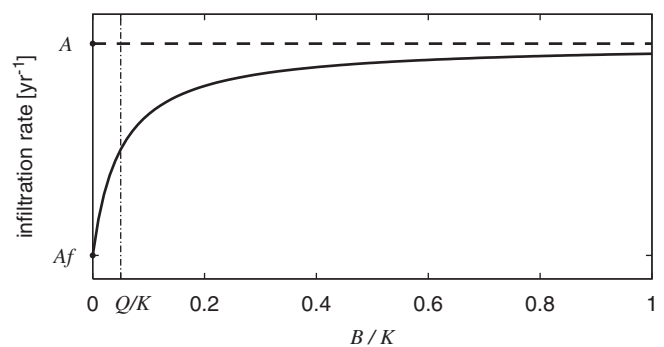

Fig. 1. The infiltration rate $I = A(B + Qf)/(B + Q)$ as a function of biomass density B. When the biomass is diminishingly small ($B \ll Q$) the infiltration rate approaches the value of Af. When the biomass is large ($B \gg Q$) the infiltration rate approaches A. The infiltration contrast between bare and vegetated soil is quantified by the parameter f, where $0 \leqslant f \leqslant 1$; when $f = 1$ the contrast is zero and when $f = 0$ the contrast is maximal. Small f values can model biological crusts which significantly reduce the infiltration rates in bare soils. Disturbances involving crust removal can be modeled by relatively high f values. The parameters used are given in Table 1.

Table 1
A list of parameters of the model, their units and their numerical values

Parameter	Units	Description	Value/range
K	kg/m^2	Maximum standing biomass	1
Q	kg/m^2	Biomass reference value beyond which infiltration rate under a patch approaches its maximum	0.05
M	yr^{-1}	Rate of biomass loss due to mortality and disturbances	1.2
A	yr^{-1}	Infiltration rate in fully vegetated soil	40
N	yr^{-1}	Soil water evaporation rate	4
E	(kg/m^2)$^{-1}$	Root's augmentation per unit biomass	3.5
Λ	(kg/m^2)$^{-1}$ yr^{-1}	Biomass growth rate per unit soil water	0.032
Γ	(kg/m^2)$^{-1}$ yr^{-1}	Soil water consumption rate per unit biomass	20
D_B	m^2/yr	Seed dispersal coefficient	6.25×10^{-4}
D_W	m^2/yr	Transport coefficient for soil water	6.25×10^{-2}
D_H	m^2/yr (kg/m^2)$^{-1}$	Bottom friction coefficient between surface water and ground surface	0.05
S_0	m	Minimal root-system size	0.125
$Z(\mathbf{X})$	mm	Topography function	
P	kg/m^2 yr^{-1}	Precipitation rate	[0, 1000]
R	–	Evaporation reduction due to shading	0.95
f	–	Infiltration contrast between bare soil and vegetated soil	0.1

The parameters values are set to represent shrubs, using Sternberg and Shoshany (2001), Hillel (1998), Rietkerk et al. (2002).

The growth rate G_B has the following non-local form:

$$G_B(\mathbf{X}, T) = \Lambda \int_\Omega G(\mathbf{X}, \mathbf{X}', T) W(\mathbf{X}', T)\, d\mathbf{X}',$$

$$G(\mathbf{X}, \mathbf{X}', T) = \frac{1}{2\pi S_0^2} \exp\left[-\frac{|\mathbf{X} - \mathbf{X}'|^2}{2[S_0(1 + EB(\mathbf{X}, T))]^2} \right], \qquad (3)$$

where Λ represents the plant's growth rate per unit amount of soil water, the Gaussian kernel $G(\mathbf{X}, \mathbf{X}', T)$ represents the root system and the integration is over the entire domain Ω.[1] According to this form, the biomass growth rate depends not only on the amount of soil water at the plant location $\mathbf{X}$, but also on the amount of soil water in the neighborhood, $\mathbf{X}'$, spanned by the plant's roots. Root augmentation in response to biomass growth is modeled by the width, $S_0(1 + EB(\mathbf{X}, T))$, of the Gaussian function in Eq. (3) which provides a measure of the root-system size. The parameter E quantifies the root augmentation per unit biomass, beyond a minimal root-system size S_0. It measures the strength of the positive uptake feedback due to root augmentation; the larger E the stronger the feedback effect.

The soil water consumption rate at a point $\mathbf{X}$ is similarly given by

$$G_W(\mathbf{X}, T) = \Gamma \int_\Omega G(\mathbf{X}', \mathbf{X}, T) B(\mathbf{X}', T)\, d\mathbf{X}', \qquad (4)$$

where Γ measures the soil water consumption rate per unit biomass. The soil water consumption rate at a given point ($\mathbf{X}$) is due to all plants (located in neighboring points $\mathbf{X}'$) whose roots extend to this point. Note that $G(\mathbf{X}', \mathbf{X}, T) \neq G(\mathbf{X}, \mathbf{X}', T)$.

The parameter values used in this paper are summarized in Table 1. They are chosen to describe shrub species and are taken or deduced from (Hillel, 1998; Sternberg and Shoshany, 2001; Rietkerk et al., 2002). The model solutions described here are robust and do not depend on delicate tuning of any particular parameter. The precipitation parameter represents mean annual rainfall in this paper and assumes constant values. This approximation is justified for species, such as woody shrubs, whose growth time-scales are much larger than the time-scale of rainfall variability.

It is advantageous to study the model equations using non-dimensional variables and parameters, for it eliminates dependent parameters and reveals the possible equivalence of different parameters in controlling the states of the system. Rescaling the model variables and parameters as in Table 2, we obtain the following non-dimensional form of the model equations:

$$b_t = G_b b(1 - b) - b + \delta_b \nabla^2 b,$$

$$w_t = \mathscr{I}h - \nu(1 - \rho b)w - G_w w + \delta_w \nabla^2 w,$$

$$h_t = p - \mathscr{I}h + \delta_h \nabla^2(h^2) + 2\delta_h \nabla h \cdot \nabla \zeta + 2\delta_h h \nabla^2 \zeta, \qquad (5)$$

where t and $\mathbf{x} = (x, y)$ are the non-dimensional time and spatial coordinates, $\nabla^2 = \partial_x^2 + \partial_y^2$ and $\mathbf{x}' = (x', y')$.

---

[1]The kernel G is normalized such that for $B = 0$ the integration over an infinite domain equals unity.

Table 2
Relations between non-dimensional variables and parameters and the dimensional ones appearing in the dimensional form of the model equations (1)–(4)

Quantity	Scaling
b	B/K
w	$\Lambda W/N$
h	$\Lambda H/N$
q	Q/K
v	N/M
α	A/M
η	EK
γ	$\Gamma K/M$
p	$\Lambda P/MN$
δ_b	D_B/MS_0^2
δ_w	D_W/MS_0^2
δ_h	$D_H N/M\Lambda S_0^2$
ζ	$\Lambda Z/N$
ρ	R
t	MT
$\mathbf{x}$	$\mathbf{X}/S_0$

The infiltration term is given by

$$\mathcal{I} = \alpha \frac{b(\mathbf{x},t) + qf}{b(\mathbf{x},t) + q}, \tag{6}$$

the growth rate term G_b is written as

$$G_b(\mathbf{x},t) = v \int_\Omega g(\mathbf{x},\mathbf{x}',t) w(\mathbf{x}',t)\, d\mathbf{x}',$$

$$g(\mathbf{x},\mathbf{x}',t) = \frac{1}{2\pi} \exp\left[-\frac{|\mathbf{x}-\mathbf{x}'|^2}{2(1+\eta b(\mathbf{x},t))^2}\right], \tag{7}$$

and similarly, the soil water consumption rate can be written as

$$G_w(\mathbf{x},t) = \gamma \int_\Omega g(\mathbf{x}',\mathbf{x},t) b(\mathbf{x}',t)\, d\mathbf{x}'. \tag{8}$$

In obtaining Eqs. (5) we eliminated four dependent parameters (K, M, Λ, S_0). The non-dimensional form of the precipitation parameter

$$p = \frac{\Lambda P}{MN}, \tag{9}$$

proves the equivalence of decreasing the precipitation rate, P, to increasing the mortality (grazing) rate, M, or the evaporation rate, N, in traversing the basic instabilities of the system. The non-dimensional precipitation p can be used to define an *aridity parameter*, $a = p^{-1}$. This form extends an earlier definition (Lefever and Lejeune, 1997) by adding the two parameters P and M.

4. Landscape states along aridity gradients

The model has two homogeneous stationary solutions representing bare soil and uniform coverage of the soil by vegetation. Their existence and linear stability ranges for plane topography are shown in the bifurcation diagrams displayed in Fig. 2. In Fig. 2D the bifurcation parameter is
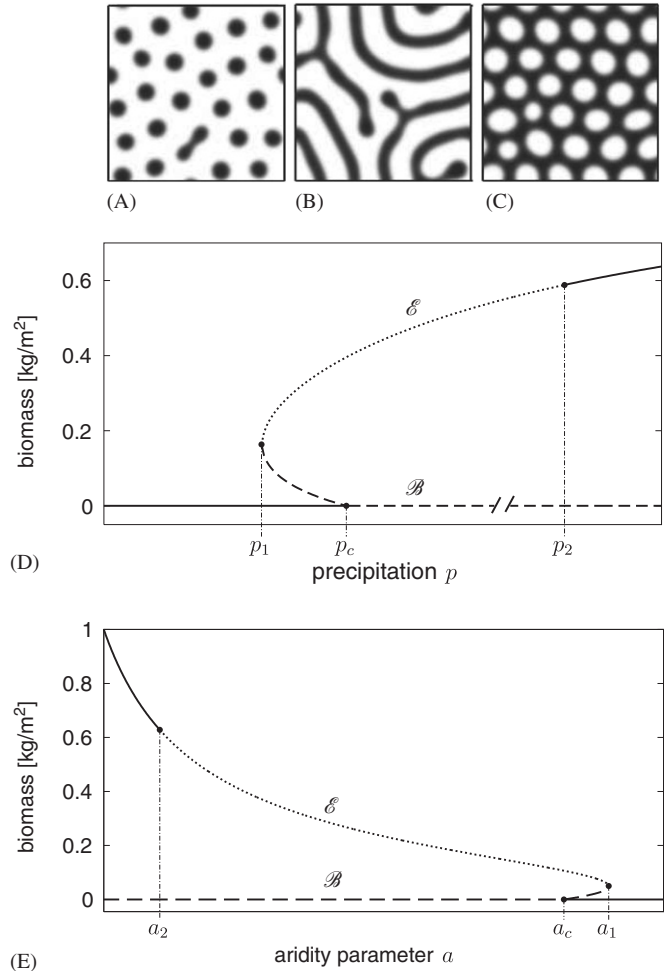

Fig. 2. Bifurcation diagrams for homogeneous stationary solutions of the model equations (Eqs. (5)–(8)) showing the biomass B vs. precipitation p (panel D) and aridity a (panel E) for plane topography. The solution branches $\mathcal{B}$ and $\mathcal{E}$ denote, respectively, the bare-soil and uniform vegetation solutions. Solid lines represent linearly stable solutions, dashed lines represent solutions which are unstable to homogeneous perturbations, and dotted line represents solutions which are stable to homogeneous perturbations but unstable to non-homogeneous ones. Also shown are the basic vegetation patterns along the precipitation gradient, spots (panel A), stripes (panel B) and gaps (panel C), obtained by numerical integration of the model equations. Dark shades of gray represent high biomass density. The same sequence of patterns but in a reverse order appears along the aridity axis. The domain size in panels (A)–(C) is $10 \times 10 \, \mathrm{m}^2$. The bifurcation points in panels D and E are: $p_c = 1.00$, $p_1 = 0.91$, $p_2 = 8.21$, $a_c = 1.00$, $a_1 = 1.10$, $a_2 = 0.12$. The parameters used are given in Table 1.

the dimensionless precipitation p. In Fig. 2E the bifurcation parameter is chosen to be the aridity parameter, a. Since $a = MN/\Lambda P$, the latter form qualitatively represents the dependence of the homogeneous solutions and their linear stabilities on the mortality rate M or the evaporation rate N. The linear stability analysis leading to this diagram is described in Appendix A.

The bare soil solution, denoted in Fig. 2 by $\mathcal{B}$, is given by $b = 0$, $w = p/v$ and $h = p/\alpha f$. It is linearly stable for $p < p_c = 1$ and it loses stability at $p = 1$ to uniform
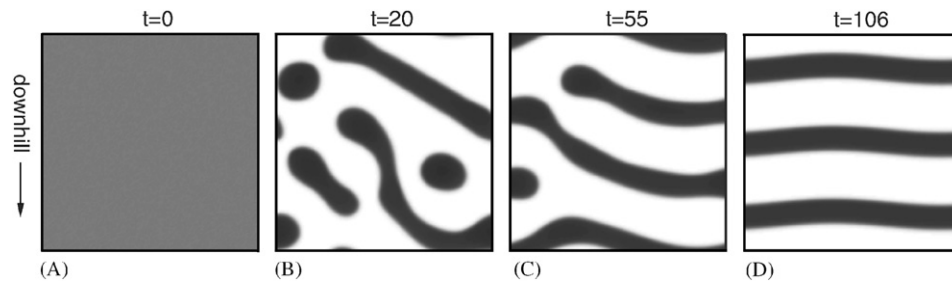
Fig. 3. Development of vegetation bands traveling uphill from an unstable uniform vegetation state, obtained by numerical integration of the model equations (Eqs. (5)–(8)) at $P = 600$ mm/yr. The different panels (A)–(D) shows snapshots of this process at different times (t is in years). Dark shades of gray represent high biomass density. The bands are oriented perpendicular to the slope gradient and travel uphill with typical speed of a few centimeters per year. The parameters used are given in Table 1, the domain size is $5 \times 5 \, m^2$ and the slope angle is $15°$.

perturbations.[2] The uniform vegetation solution, denoted by $\mathscr{E}$, exists for $p > 1$ in the case of a supercritical bifurcation and for $p > p_1$ (where $p_1 < 1$) in the case of a subcritical bifurcation. It is stable, however, only beyond another threshold, $p = p_2 > p_1$. As p is decreased below p_2 the uniform vegetation solution loses stability to non-uniform perturbations in a finite wave number (Turing like) instability (Cross and Hohenberg, 1993). These perturbations grow to form large amplitude patterns. The following sequence of basic patterns has been found at decreasing precipitation values for plane topography (see panels A–C in Fig. 2): gaps, stripes and spots. The sequence of basic landscape states, uniform vegetation, gaps, stripes, spots and bare soil, as the precipitation parameter is decreased, has been found in earlier vegetation models (Lefever et al., 2000; von Hardenberg et al., 2001; Okayasu and Aizawa, 2001; Rietkerk et al., 2002; Gilad et al., 2004).

Any pair of consecutive landscape states along the rainfall (precipitation) gradient has a range of bistability (coexistence of two stable states): bistability of bare soil with spots, spots with stripes, stripes with gaps, and gaps with uniform vegetation. Bistability of different landscape states has at least three important implications: (i) it implies hysteresis, which has been used to elucidate the irreversibility of desertification phenomena (Rietkerk and van de Koppel, 1997; Rietkerk et al., 1997; von Hardenberg et al., 2001; Scheffer et al., 2001), (ii) it implies vulnerability to desertification by disturbances involving biomass removal, and (iii) it increases landscape diversity as patterns involving spatial mixtures of two distinct landscape states become feasible.

The basic landscape states persist on slopes with two major differences: stripes, which form labyrinthine patterns on a plane, reorient perpendicular to the slope direction to form parallel bands, and the patterns travel uphill (typical speeds for the parameters used in this paper are of the order of centimeters per year). Fig. 3 shows the development of bands traveling uphill from an unstable uniform vegetation state. Traveling bands on a slope have been found in earlier models as well (Thiéry et al., 1995; Lefever

and Lejeune, 1997; Dunkerley, 1997; Klausmeier, 1999; von Hardenberg et al., 2001; Okayasu and Aizawa, 2001; Rietkerk et al., 2002; Gilad et al., 2004). Another difference is the coexistence of multiple band solutions with different wave numbers in wide precipitation ranges (Yizhaq et al., 2005). The landscape states on plane and slope topographies predicted by this and earlier models are consistent with field observations (Valentin et al., 1999; Rietkerk et al., 2004; Lejeune et al., 2004).

5. Ecosystem engineering

Throughout this paper we define engineering as the capacity of a plant species to concentrate soil water beyond the level pertaining to bare soil. The concentration process can be due to an increased infiltration rate at the plant patch, or due to runoff interception by the soil mound the plant forms. To simulate the former process we need to choose small f values. To simulate the latter process a topography function (ζ) that mimics soil mounds should be chosen. For simplicity we study the former process.

5.1. The engineering–resilience trade-off

We study engineering by varying the parameters f and η (the non-dimensional form of E) that controls the infiltration feedback and the uptake feedback (due to root augmentation), respectively. We look for conditions that maximize the engineering capacity and ask what is the price the system has to pay for attaining high engineering. The results are summarized in Fig. 4 and indicate the existence of a trade-off between the engineering capacity of a plant and its resilience to disturbances[3]; conditions that favor ecosystem engineering, resulting in water-enriched patches or micro-habitats, imply low resilience, and conditions that favor high resilience imply weak or no engineering.

Shown in Fig. 4 are spatial profiles of b, w and h for a single patch of the ecosystem engineer at decreasing values

---

[2]The bifurcation is subcritical (supercritical) depending whether the quantity $2\eta v/[v(1 - \rho) + \gamma]$ is greater (lower) than unity.

[3]Resilience in this paper is defined as the ability of a system to recover from a disturbance. It differs from the concept of "linear stability" in that the disturbance can be strong and lead the system through a long transient of different states before the system recovers.
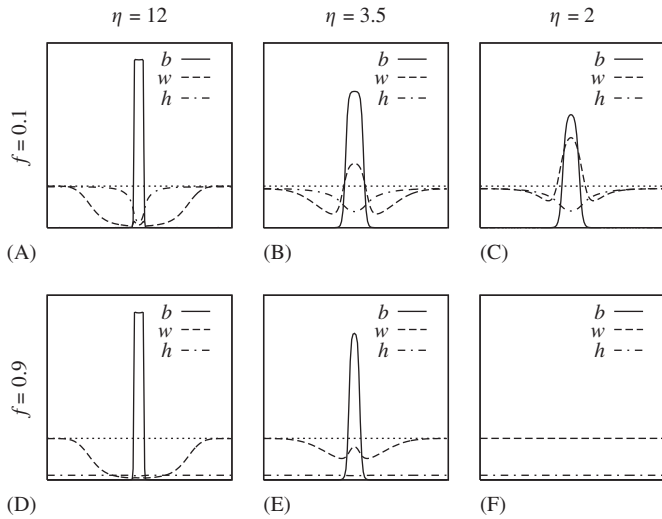
Fig. 4. Spatial profiles of the variables b, w and h as affected by the parameters that control the main positive biomass-water feedbacks, f (infiltration feedback) and η (uptake feedback). The profiles are cross-sections of two-dimensional simulations of the model equations (Eqs. (5)–(8)). In all panels, the horizontal dotted lines denote the soil-water level at bare soil. Strong infiltration feedback and weak uptake feedback (panel C) leads to high soil-water concentration reflecting strong engineering. Strong uptake feedback results in soil-water depletion and no engineering, irrespective of the infiltration-feedback strength (panels A,D). While the species characterized by $\eta = 2$ is the best engineer under conditions of strong infiltration contrast (panel C), it leads to low system resilience; the engineer along with the micro-habitat it forms completely disappear when the infiltration contrast is strongly reduced, e.g. by crust removal (panel F). A species with somewhat stronger uptake feedback ($\eta = 3.5$) still acts as an ecosystem engineer (panel B) and also survives disturbances that reduce the infiltration contrast (panel E), thereby retaining the system's resilience. Parameter values are given in Table 1 with $P = 75 \, \text{mm/yr}$. Panels (A) and (D) span a horizontal range of 14 m while all other panels span 3.5 m. The vertical range in all panels is $[0, 1] \, \text{kg/m}^2$ for the biomass density, and $[0, 187.5] \, \text{kg/m}^2$ for the soil-water density.

of η, representing species with different root augmentation properties, and for two extreme values of f. The value $f = 0.1$ models high infiltration rates under engineer's patches and low infiltration rates in bare soil, which may result from a biological crust covering the bare soil. The value $f = 0.9$ models high infiltration rates everywhere. This case may describe, for example, un-crusted sandy soil. Engineering effects resulting in soil water concentration appear only in the case of (i) low infiltration in bare soil, (ii) engineer species with limited root augmentation capabilities, $\eta = 3.5, \eta = 2$ (panels B and C in Fig. 4). The soil water density under an engineer's patch in this case exceeds the soil-water density level of bare soil (shown by the dotted lines), thus creating opportunities for species that require this extra amount of soil water to colonize the water-enriched patch.

While a weak uptake feedback enhances the engineering ability, it reduces the resilience of the ecosystem engineer (and all dependent species) to disturbances. Fig. 4F shows the response of an engineer species with the highest engineering ability to concentrate water ($\eta = 2$, Fig. 4C)

to a disturbance that strongly reduces the infiltration contrast ($f = 0.9$). In the following we refer to crust removal, but other disturbances that reduce the infiltration contrast, such as erosion of bare soil, will have similar effects. The engineer, and consequently the micro-habitat it forms, disappear altogether for two reasons: (i) surface water infiltrates equally well everywhere and the plant patch is no longer effective in trapping water, (ii) the engineer's roots are too short to collect water from the surrounding area.

Resilient ecosystem engineers are obtained with strong infiltration feedbacks and moderate uptake feedbacks ($\eta = 3.5$) as Fig. 4E shows. Removal of the crust (by increasing f) destroys the micro-habitats (soil-water density is smaller than the bare-soil's value) but the engineer persists. Once the crust recovers the ecosystem engineer resumes its capability to concentrate water and the micro-habitats recover as well. It is also of interest to comment that when the uptake feedback is too strong, the plant persists but it no longer functions as an ecosystem engineer (Fig. 4A,D).

Fig. 5 provides another view of the engineering–resilience trade-off. Shown in this figure are two graphs of the maximum soil-water density under an engineer patch as a function of the coverage of the surrounding crust, which is parameterized by f. A plant with high engineering strength ($\eta = 2$) has low resilience to disturbances that reduce the infiltration contrast (increase f), e.g. crust removal. As f increases past a critical value f_c the engineer patch disappears altogether, leaving behind a bare soil with no water enriched patches and no ability for the system to
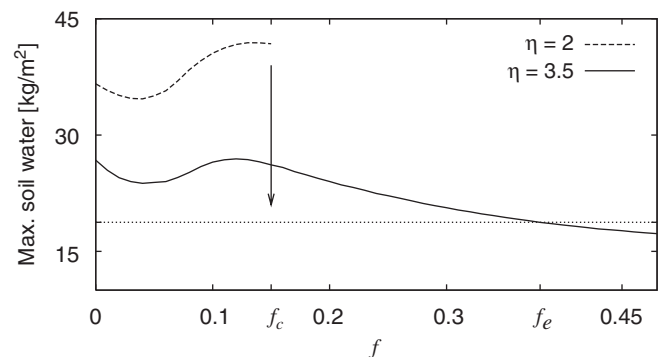

Fig. 5. Maximal soil-water densities under ecosystem-engineer patches for two different engineer species, $\eta = 2$ (dashed curve) and $\eta = 3.5$ (solid curve), as functions of the infiltration contrast, quantified by f. At low values of f (e.g. in the presence of a soil crust) both species concentrate the soil-water resource under their patches beyond the soil-water level of bare soil (horizontal dotted line), thereby creating water enriched micro-habitats for other species (see Fig. 4). The engineer species with $\eta = 2$ outperforms the $\eta = 3.5$ species, but does not survive low infiltration contrasts (resulting e.g. from crust removal); as f exceeds a threshold value, $f_c = 0.15$, the engineer's patch dries out and the micro-habitat it forms is irreversibly destroyed. The $\eta = 3.5$ species, on the other hand, survives low infiltration contrasts and while its engineering capacity disappears above a second threshold $f_e = 0.38$, the engineering capacity is regained as the infiltration contrast builds up (e.g. by crust recovery). Parameter values are given in Table 1 with $P = 75 \, \text{mm/yr}$.

recover (arrow pointing downwards). In contrast, a plant with lower engineering strength ($\eta = 3.5$) survives severe reduction of the infiltration contrast. The engineering effect no longer exists for $f > f_e$, but once the disturbances disappear and the infiltration contrast builds up again, engineering resumes.

5.2. Engineering niches

The next question we address is what forms of engineering at the single patch level can be expected, and what types of niches or micro-habitats they create? Model simulations suggest the existence of two basic engineering forms as shown in Fig. 6: a hump-shaped form, where the maximum of the soil-water distribution occurs at the center of the patch, and a ring-shaped form, where the soil-water maximum is along the circumference of the patch. The ring-shaped form is associated with bigger biomass patches and can be obtained from a hump-shaped form by increasing the precipitation rate or the infiltration contrast. This results in outward expansion of the biomass patch and increased competition over the water resource at the patch center, followed by soil-water depletion.

The two soil-water distributions represent different niches for herbaceous species. Species in need for abundant sunlight will favor ring-shaped distributions along which the shading is weak. Species sensitive to grazing, on the other hand, will prefer hump-shaped distributions where the water-rich regions are protected by the engineer canopies.

5.3. Local engineering by global pattern changes

The water-biomass feedbacks induce intraspecific competition at the single patch scale which leads to spatial patterning (or self-organized patchiness; Rietkerk et al., 2004) at the landscape scale. Are there landscape processes that feedback to the level of a single patch? Studies of the model indeed suggest that such processes can exist; global landscape transitions from one vegetation pattern to another can affect engineering at the single patch level.

The example we study pertains to vegetation patterns on a slope, and to a parameter regime where a stable banded pattern coexists with a stable spotted pattern. The banded pattern is locally disturbed by removing the biomass of a small band segment as shown in Fig. 7A. This disturbance induces a chain process downhill that culminates in a transition to a spotted pattern as Figs. 7B–D show. The biomass removal at the uppermost band allows for more runoff to accumulate at the band segment just below it. As a result this segment grows faster, draws more water from its surrounding and induces vegetation decay at the nearby band segments. The decay of the vegetation in the nearby segments allow for more runoff to accumulate at the next band downhill. The whole process continues repeatedly until the whole pattern transforms into a spot pattern.

The lower panels in Fig. 7 show the soil-water distributions along the transects denoted by the dashed lines in the upper panels. The transition to spots is accompanied by increased engineering; the soil-water density under a spot is significantly higher than the density under a band. The mechanism of this behavior can be understood as follows. The spot pattern self-organizes to form an hexagonal pattern. As a result each spot experiences a bare area uphill which is twice as large as the bare area between successive bands, and therefore absorbs more runoff. In addition, the higher biomass density of spots (due to water uptake from all directions) increases the infiltration contrast.

6. Discussion

We present here a spatially explicit mathematical model for plants as ecosystem engineers. Earlier models of vegetation pattern formation (Rietkerk et al., 2004) consider water uptake as a local negative-feedback process between biomass and water. The present model goes one step further in capturing the non-local nature of the water-uptake process and the augmentation of the root system in response to (over-ground) biomass growth. This aspect of the water-uptake process implies positive feedback relationships between biomass and water which can be understood as follows. As the biomass grows, the root
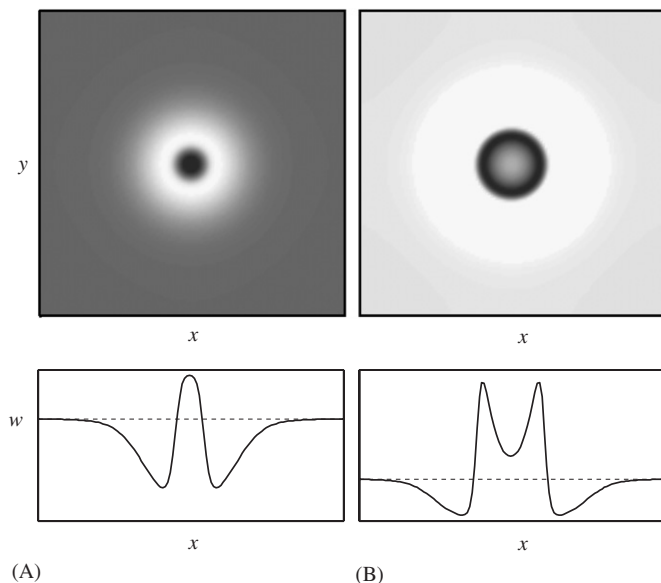

Fig. 6. Two typical spatial distributions of soil water at the scale of a single patch, obtained with different infiltration rates in bare soil. The upper panels show two-dimensional soil water distributions (dark shades of gray represent high soil-water densities), while the lower panels show the corresponding one-dimensional cross-sections along the patch center. In the range of intermediate to low infiltration rates (panel A, $f = 0.1$) the soil-water density is maximal at the center of the patch, whereas at very low infiltration rates (panel B, $f = 0.01$) the maximum is shifted to the edge of the patch. Similar soil water distributions can be obtained at different precipitation values. The soil-water distributions were obtained by numerical integration of the model equations (Eqs. (5)–(8)) at $P = 75$ mm/yr, with domain size of 5×5 m^2. All other parameters are given in Table 1.
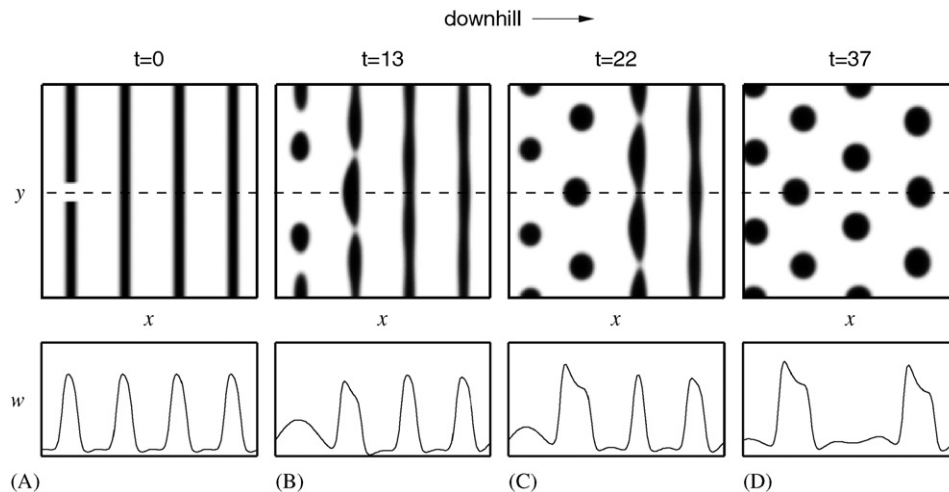
Fig. 7. A pattern transition at the landscape level from bands to spots affects engineering at the single patch level. The transition is induced by a local clear-cutting disturbance (leftmost band in panel A), and is shown in panels A–D by displaying snapshots of biomass patterns (darker gray shades correspond to higher biomass density) at successive times (t is in years). The patterns were obtained by solving numerically Eqs. (5)–(8) at a fixed precipitation value where both band and spot patterns are stable. The initial cut of the uppermost band induces a chain response culminating in an hexagonal spot pattern. The lower panels show soil water profiles along the transects denoted by the dashed lines in the corresponding upper panels. The soil-water density under spots is higher than the density under bands despite the fixed environmental conditions. Domain size is $5 \times 5\,\mathrm{m}^2$, $P = 240\,\mathrm{mm/yr}$, slope angle is $15°$ and all other parameters are given in Table 1.

system extends its size and probes new soil regions. Water uptake from these regions further accelerates the biomass growth.

Both the water-uptake feedback (as modeled here) and the infiltration feedback, independently of one another, lead to similar vegetation patterns at the landscape level. However, they imply different engineering and resilience properties. Dominance of the infiltration feedback leads to strong engineering and low resilience, whereas dominance of the uptake feedback leads to no engineering (or "negative" engineering; Jones et al., 1997) and high resilience.

The trade-off between engineering and resilience, as the relative strength of the two feedbacks changes, is significant for understanding the stability and functioning of water-limited ecosystems on micro (patch) and macro (watershed) spatial scales (Shachak et al., 1998). The soil-moisture accumulation at an engineer patch accelerates litter decomposition and nutrient production, and culminates in the formation of fertility islands. Watershed-scale disturbances that are incompatible with the resilience of dominant engineer species can destroy the engineer patches and the fertility islands associated with them, thereby damaging the stability and functioning of the ecosystem.

We further found that environmental conditions that affect the engineer patch size can modify the soil-water distribution under the engineer's patch and thus the micro-habitat it creates. We demonstrated a transition from a hump-shaped distribution to a ring-shaped distribution by increasing the infiltration contrast (decreasing f), but similar transitions can be obtained in the model by changing other parameters, e.g. increasing the precipitation rate, P, decreasing the evaporation rate, N, or decreasing the grazing stress, M.

We also studied possible effects of pattern transitions at the landscape level on engineering at the single patch level. We found that a global transition from vegetation bands to spots on a slope can result in stronger local engineering, suggesting that studies of single-patch dynamics should not be confined to the patch level alone. This effect is tightly related to the hexagonal structure of the spot pattern (any spot has six neighbor spots), where the distance between any adjacent spots along the slope direction is about twice as large as the distance between two adjacent bands. In heterogeneous systems (containing e.g. rocky or eroded soil parts) the spot pattern will generally appear disordered, but the basic principle leading to enhanced engineering still holds because of the reduced patch connectivity in spotted patterns as compared with banded patterns and the resulting higher runoff accumulation at vegetation patches.

We restricted our analysis to the rather artificial circumstances of homogeneous systems with respect to soil properties, topography, rainfall, evaporation, mortality, etc. We did so to highlight the roles of self-organizing patterns of biomass and soil water in breaking the spatial symmetry of the system and in creating habitats. Heterogeneous factors, as well as temporal rainfall variability, can be incorporated into the model by introducing time and space dependent parameters.

The model in its present form takes into account the major feedbacks between vegetation and water but leaves out a few other feedbacks. The atmosphere affects vegetation through the precipitation and evaporation rate parameters, but the vegetation is assumed to have no feedback on the atmosphere. Organic nutrients effects are parameterized by the biomass growth rate, but litter decomposition (Moro et al., 1997) that feedbacks on nutrient concentrations is not considered. Finally, ground

topography, parameterized by the function $\zeta(\mathbf{x})$, affects runoff and water concentration, but topography changes due to soil erosion by water flow are neglected. These simplifications restrict the circumstances the model applies to.

Another limitation of the model is the elimination of the soil depth dimension which restricts the variety of roots effects the model can capture. Thus, engineering by hydraulic lifts (Caldwell et al., 1998) is not captured by the model. Finally, plant recruitment and growth are lumped together in a single biomass equation with a diffusion term modeling local seed dispersal. This modeling form rules out long-distance dispersion, e.g. by wind, water flow or animals, and seed predation, e.g. by insects or birds (Nathan and Casagrandi, 2004).

While extensions of the model to include the factors discussed above are interesting and significant, they may require considerable modifications of the model. A more direct extension of the model, that is already underway, is the inclusion of additional biomass variables representing herbaceous species which benefit from the habitats created by the ecosystem engineer. Each additional species is modeled by a biomass equation similar to that of the engineer but differing in the values of various species parameters such as growth rate, mortality and maximum standing biomass. Including in the model a second biomass variable, representing an herbaceous species, can be used to study transitions between competition and facilitation along aridity gradients (Pugnaire and Luque, 2001), and to possibly shed light on observational conflicts (Maestre et al., 2005). Including two herbaceous species can be used to study trade-offs and species-coexistence mechanisms associated with self-organized heterogeneities induced by patterns of the ecosystem engineer.

Acknowledgments

Appendix A. Linear stability analysis

We study here the linear stability of stationary homogeneous solutions of the model equations (5) to non-uniform infinitesimal perturbations, confining ourselves to plane topography. Denoting a stationary homogeneous solution by the column vector $\mathbf{U}_0 = (b_0, w_0, h_0)^{\mathrm{T}}$, we consider a perturbed solution in the form

$$\mathbf{U}(\mathbf{x}, t) = \mathbf{U}_0 + \delta\mathbf{U}(\mathbf{x}, t), \tag{A.1}$$

where

$$\delta\mathbf{U}(\mathbf{x}, t) = \mathbf{a}(t)e^{i\mathbf{k}\cdot\mathbf{x}} + c.c., \tag{A.2}$$

and $\mathbf{k}$ is the wave vector of the perturbation. In (A.1) and (A.2), $\mathbf{U} = (b, w, h)^{\mathrm{T}}$, $\delta\mathbf{U} = (\delta b, \delta w, \delta h)^{\mathrm{T}}$, $\mathbf{a} = (a_b, a_w, a_h)^{\mathrm{T}}$

and "c.c." stands for the complex conjugate. Substitution of the perturbed solution (A.1) into the model equations (5) gives

$$(\delta b)_t = G_b|_{\mathbf{U}_0+\delta\mathbf{U}}(b_0 + \delta b)[1 - (b_0 + \delta b)] - (b_0 + \delta b) + \delta_b\nabla^2(\delta b),$$

$$(\delta w)_t = \mathscr{I}|_{\mathbf{U}_0+\delta\mathbf{U}}(h_0 + \delta h) - \nu[1 - \rho(b_0 + \delta b)](w_0 + \delta w) - G_w|_{\mathbf{U}_0+\delta\mathbf{U}}(w_0 + \delta w) + \delta_w\nabla^2(\delta w),$$

$$(\delta h)_t = p - \mathscr{I}|_{\mathbf{U}_0+\delta\mathbf{U}}(h_0 + \delta h) + \delta_h\nabla^2[(h_0 + \delta h)^2], \tag{A.3}$$

where the infiltration term (see Eq. (6)) reads

$$\mathscr{I}|_{\mathbf{U}_0+\delta\mathbf{U}} = \frac{b_0 + qf + \delta b}{b_0 + q + \delta b}$$
$$= \frac{b_0 + qf}{b_0 + q} + \frac{q(1 - f)}{(b_0 + q)^2}\delta b + \mathscr{O}(\delta b^2), \tag{A.4}$$

and $\mathscr{O}(\delta b^2)$ represents terms of order two and higher in δb.

In order to evaluate the terms $G_b|_{\mathbf{U}_0+\delta\mathbf{U}}$ and $G_w|_{\mathbf{U}_0+\delta\mathbf{U}}$ we expand the kernels, as defined in Eq. (7), up to first order in δb:

$$g(\mathbf{x}, \mathbf{x}') = g^0(\mathbf{x}, \mathbf{x}') + g^1(\mathbf{x}, \mathbf{x}')\delta b(\mathbf{x}) + \mathscr{O}(\delta b^2),$$
$$g(\mathbf{x}', \mathbf{x}) = g^0(\mathbf{x}', \mathbf{x}) + g^1(\mathbf{x}', \mathbf{x})\delta b(\mathbf{x}') + \mathscr{O}(\delta b^2), \tag{A.5}$$

where

$$g^0(\mathbf{x}, \mathbf{x}') = g^0(\mathbf{x}', \mathbf{x}) = g(\mathbf{x}, \mathbf{x}')|_{b=b_0} = \frac{1}{2\pi}e^{-|\mathbf{x}-\mathbf{x}'|^2/2\sigma^2},$$

$$g^1(\mathbf{x}, \mathbf{x}') = g^1(\mathbf{x}', \mathbf{x}) = \frac{\partial}{\partial b}[g(\mathbf{x}, \mathbf{x}')]\bigg|_{b=b_0}$$
$$= \frac{\eta}{2\pi\sigma^3}|\mathbf{x} - \mathbf{x}'|^2 e^{-|\mathbf{x}-\mathbf{x}'|^2/2\sigma^2}. \tag{A.6}$$

Here, $\sigma \equiv 1 + \eta b_0$ and $|\mathbf{x} - \mathbf{x}'|^2 = (x - x')^2 + (y - y')^2$.

Substituting these forms and the perturbed solution in (7), we obtain up to first order

$$G_b|_{\mathbf{U}_0+\delta\mathbf{U}} = \nu \int g(\mathbf{x}, \mathbf{x}')w(\mathbf{x}')\,\mathrm{d}\mathbf{x}'$$
$$\approx \nu \int [g^0(\mathbf{x}, \mathbf{x}') + g^1(\mathbf{x}, \mathbf{x}')\delta b(\mathbf{x})][w_0 + \delta w(\mathbf{x}')]\,\mathrm{d}\mathbf{x}'$$
$$= \nu w_0 \int g^0(\mathbf{x}, \mathbf{x}')\,\mathrm{d}\mathbf{x}' + \nu \int g^0(\mathbf{x}, \mathbf{x}')\delta w(\mathbf{x}')\,\mathrm{d}\mathbf{x}'$$
$$+ \nu w_0\delta b(\mathbf{x}) \int g^1(\mathbf{x}, \mathbf{x}')\,\mathrm{d}\mathbf{x}', \tag{A.7}$$

where the integration is over the entire domain. Solving the integrals in Eq. (A.7) results in the following expression for $G_b|_{\mathbf{U}_0+\delta\mathbf{U}}$,

$$G_b|_{\mathbf{U}_0+\delta\mathbf{U}} = \nu w_0\sigma^2 + \nu\sigma^2 e^{-k^2\sigma^2/2}\delta w(\mathbf{x}) + 2\nu\eta\sigma w_0\delta b(\mathbf{x}), \tag{A.8}$$

where $k = |\mathbf{k}|$ is the perturbation's wave number. Applying the same procedure to $G_w|_{\mathbf{U}_0+\delta\mathbf{U}}$ using Eq. (8) we get

$$G_w|_{\mathbf{U}_0+\delta\mathbf{U}} = \gamma b_0\sigma^2 + \gamma\sigma e^{-k^2\sigma^2/2}[1 + \eta b_0(3 - \sigma^2 k^2)]\delta b(\mathbf{x}). \tag{A.9}$$

Substituting Eqs. (A.4), (A.8) and (A.9) into Eq. (A.3), keeping terms to first order only, and using the fact that the stationary homogeneous solutions satisfy

$$0 = v b_0(1 - b_0)(1 + \eta b_0)^2 w_0 - b_0, \tag{A.10}$$

$$0 = \alpha h_0\frac{b_0 + qf}{b_0 + q} - v(1 - \rho b_0)w_0 - \gamma w_0 b_0(1 + \eta b_0)^2, \tag{A.11}$$

$$0 = p - \alpha h_0\frac{b_0 + qf}{b_0 + q}, \tag{A.12}$$

we obtain the following system of linear ordinary differential equations for the perturbation amplitudes $\mathbf{a}(t)$:

$$\frac{d\mathbf{a}}{dt} = \mathscr{J}(k)\mathbf{a}, \tag{A.13}$$

where $\mathscr{J}(k) \in \mathbb{R}^{3\times3}$ is the Jacobian matrix whose elements are given by

$$\mathscr{J}_{11} = \sigma v w_0[1 - 2b_0 + \eta b_0(3 - 4b_0)] - 1 - \delta_b k^2,$$

$$\mathscr{J}_{12} = v b_0(1 - b_0)\sigma^2 e^{-k^2\sigma^2/2},$$

$$\mathscr{J}_{13} = 0,$$

$$\mathscr{J}_{21} = \alpha h_0\frac{q(1 - f)}{(b_0 + q)^2} + \rho v w_0$$
$$\quad - \gamma w_0\sigma e^{-k^2\sigma^2/2}[1 + \eta b_0(3 - \sigma^2 k^2)],$$

$$\mathscr{J}_{22} = -v(1 - \rho b_0) - \gamma b_0\sigma^2 - \delta_w k^2,$$

$$\mathscr{J}_{23} = \alpha\frac{b_0 + qf}{b_0 + q},$$

$$\mathscr{J}_{31} = -\alpha h_0\frac{q(1 - f)}{(b_0 + q)^2},$$

$$\mathscr{J}_{32} = 0,$$

$$\mathscr{J}_{33} = -\alpha\frac{b_0 + qf}{b_0 + q} - 2\delta_h h_0 k^2. \tag{A.14}$$

Assuming exponential growth for the perturbation amplitudes, $\mathbf{a}(t) = \mathbf{a}(0)e^{\lambda t}$, we obtain the eigenvalue problem

$$\mathscr{J}(k)\mathbf{a} = \lambda\mathbf{a}, \tag{A.15}$$

whose solution gives dispersion relations of the form $\lambda = \lambda(k)$. These relations provide information about the stability of stationary homogeneous solutions, for the growth rate of a perturbation characterized by a wave number k is given by the largest real part of $\lambda(k)$. Fig. 8 shows growth rate curves calculated for a uniform vegetation state around the instability point $p = p_2$ of this state.
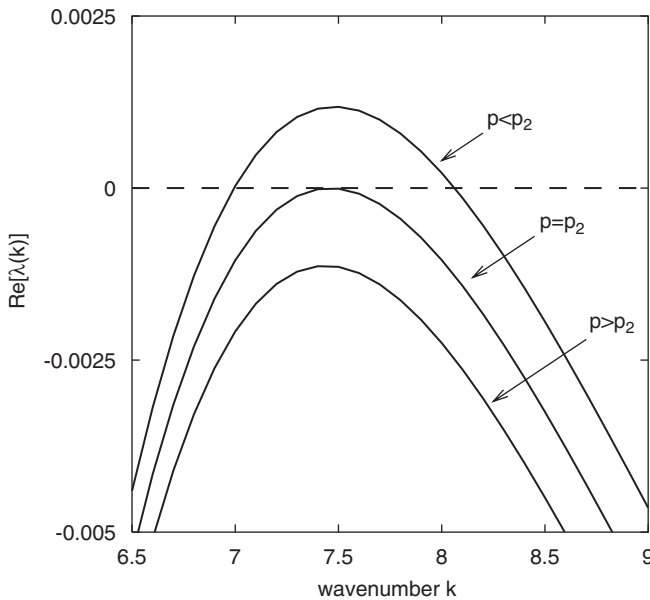

Fig. 8. Growth-rate curves for non-homogeneous spatial perturbations of the uniform vegetation solution of the model equations Eqs. (5)–(8) (denoted by $\mathscr{E}$ in Fig. 2), around the point $p = p_2$. When $p > p_2$ all wave numbers have negative growth rates and any perturbation decays. At $p = p_2$ a critical wave number becomes marginal; perturbations having this wave number neither grow nor decay. When $p < p_2$ there exists a band of wave numbers with positive growth rates; the uniform solution is unstable and perturbations characterized by the critical wave number grow faster than all others.

References

Boeken, B., Shachak, M., 1994. Desert plant communities in human made patches—implications for management. Ecol. Appl. 4, 702–716.

Caldwell, M.M., Dawson, T.E., Richards, J.H., 1998. Hydraulic lift: consequences of water efflux for the roots of plants. Oecologia 113, 151–161.

Campbell, S.E., Seeler, J.S., Glolubic, S., 1989. Desert crust formation and soil stabilization. Arid Soil Res. Rehabil. 3, 217–228.

Charley, J., West, N., 1975. Plant-induced soil chemical patterns in some shrub-dominated semi-desert ecosystems in Utah. J. Ecol. 63, 945–963.

Cross, M.C., Hohenberg, P.C., 1993. Pattern formation outside of equilibrium. Rev. Mod. Phys. 65, 851–1112.

Dunkerley, D.L., 1997. Banded vegetation: development under uniform rainfall from a simple cellular automaton model. Plant Ecol. 129, 103–111.

Gilad, E., von Hardenberg, J., Provenzale, A., Shachak, M., Meron, E., 2004. Ecosystem engineers: from pattern formation to habitat creation. Phys. Rev. Lett. 93, 0981051.

Gurney, W.S.C., Lawton, J.H., 1996. The population dynamics of ecosystem engineers. Oikos 76, 273–283.

Hillel, D., 1998. Environmental Soil Physics. Academic Press, San Diego.

HilleRisLambers, R., Rietkerk, M., Van den Bosch, F., Prins, H.H.T., de Kroon, H., 2001. Vegetation pattern formation in semi-arid grazing systems. Ecology 82, 50–61.

Jones, C.G., Lawton, J.H., Shachak, M., 1994. Organisms as ecosystem engineers. Oikos 69, 373–386.

Jones, C.G., Lawton, J.H., Shachak, M., 1997. Positive and negative effects of organisms as ecosystem engineers. Ecology 78, 1946–1957.

Klausmeier, C.A., 1999. Regular and irregular patterns in semiarid vegetation. Science 284, 1826–1828.

Laland, K.N., Odling-Smee, F.J., Feldman, M.W., 1999. Evolutionary consequences of niche construction and their implications for ecology. Proc. Natl Acad. Sci. 96, 10242–10247.

Lefever, R., Lejeune, O., 1997. On the origin of tiger bush. Bull. Math. Biol. 59, 263–294.

Lefever, R., Lejeune, O., Couteron, P., 2000. Generic modelling of vegetation patterns. A case study of tiger bush in sub-Saharian Sahel. In: Maini, P.K., Othmer, H.G. (Eds.), Mathematical Models for Biological Pattern Formation, IMA Volumes in Mathematics and its Applications, vol. 121. Springer, New York, pp. 83–112.

Lejeune, O., Tlidi, M., Lefever, R., 2004. Vegetation spots and stripes: dissipative structures in arid landscapes. Int. J. Quantum Chem. 98, 261–271.

Maestre, F.T., Valladares, F., Reynolds, J.F., 2005. Is the change of plant–plant interactions with abiotic stress predictable? A meta-analysis of field results in arid environments. J. Ecol. 93, 748–757.

Meron, E., Gilad, E., von Hardenberg, J., Shachak, M., Zarmi, Y., 2004. Vegetation patterns along a rainfall gradient. Chaos, Solitons Fractals 19, 367–376.

Moro, M.J., Pugnaire, F.I., Haase, P., Puigdefabregas, J., 1997. Mechanisms of interaction between *Retama sphaerocarpa* and its understorey layer in a semiarid environment. Ecography 20, 175–184.

Murray, J.D., 1993. Mathematical Biology, Second Corrected Ed. (Biomathematics, vol. 19). Springer, Berlin, Heidelberg.

Nathan, R., Casagrandi, R., 2004. A simple mechanistic model of seed dispersal, predation and plant establishment: Janzen–Connell and beyond. J. Ecol. 92, 733–746.

Odling-Smee, F.J., 1988. Niche-constructing phenotypes. In: Plotkin, H.C. (Ed.), The Role of Behavior in Evolution. MIT Press, Cambridge, MA.

Odling-Smee, F.J., Laland, K.N., Feldman, M.W., 2003. Niche construction: the neglected process in evolution. Monographs in Population Biology, vol. 37. Princeton University Press.

Okayasu, T., Aizawa, Y., 2001. Systematic analysis of periodic vegetation patterns. Prog. Theor. Phys. 106, 705–720.

Perry, D.A., 1998. The scientific basis of forestry. Annu. Rev. Ecol. Syst. 29, 435–466.

Power, M.E., Tilman, D., Estes, J.A., Menge, B.A., Bond, W.J., Mills, L.S., Daily, G., Castilla, J.C., Lubchenco, J., Paine, R.T., 1996. Challenges in the quest for keystones. Bioscience 46, 609–620.

Pugnaire, F.I., Luque, M.T., 2001. Changes in plant interactions along a gradient of environmental stress. Oikos 93, 42–49.

Rietkerk, M., van de Koppel, J., 1997. Alternate stable states and threshold effects in semi-arid grazing systems. Oikos 79, 69–76.

Rietkerk, M., van den Bosch, F., van de Koppel, J., 1997. Site-specific properties and irreversible vegetation changes in semi-arid grazing systems. Oikos 80, 241–252.

Rietkerk, M., Boerlijst, M.C., van Langevelde, F., HilleRisLambers, R., van de Koppel, J., Kumar, L., Prins, H.H.T., De Roos, A.M., 2002. Self-organization of vegetation in arid ecosystems. Am. Nat. 160, 524–530.

Rietkerk, M., Dekker, S.C., de Ruiter, P.C., van de Koppel, J., 2004. Self-organized patchiness and catastrophic shifts in ecosystems. Science 305, 1926–1929.

Scheffer, M., Carpenter, S., Foley, J.A., Folke, C., Walkerk, B., 2001. Catastrophic shifts in ecosystems. Nature 413, 591–596.

Shachak, M., Jones, C.G., 1995. Ecological flow chains and ecological systems: concepts for linking species and ecosystem perspectives. In: Jones, C.G., Lawton, J.H. (Eds.), Linking Species and Ecosystems. Chapman & Hall, New York, pp. 280–294.

Shachak, M., Sachs, M., Moshe, I., 1998. Ecosystem management of desertified shrublands in Israel. Ecosystems 1, 475–483.

Shachak, M., Gosz, J., Pickett, S.T.A., Perevolotsky, A., 2005. Toward a unified framework for biodiversity studies. In: Shachak, M., Gosz, J., Pickett, S.T.A., Perevolotsky, A. (Eds.), Biodiversity in Drylands: Towards a Unified Framework. Oxford University Press, Oxford, pp. 3–14.

Shnerb, N.M., Sarah, P., Lavee, H., Solomon, S., 2003. Reactive glass and vegetation patterns. Phys. Rev. Lett. 90, 0381011.

Sternberg, M., Shoshany, M., 2001. Influence of slope aspect on Mediterranean woody formation: comparison of a semiarid and an arid site in Israel. Ecol. Res. 16, 335–345.

Thiéry, J.M., d'Herbés, J.M., Valentin, C., 1995. A model simulating the genesis of banded vegetation patterns in Niger. J. Ecol. 83, 497–507.

Valentin, C., d'Herbès, J.M., Poesen, J., 1999. Soil and water components of banded vegetation patterns. Catena 37, 1–24.

von Hardenberg, J., Meron, E., Shachak, M., Zarmi, Y., 2001. Diversity of vegetation patterns and desertification. Phys. Rev. Lett. 87, 198101.

Walker, B.H., Ludwig, D., Holling, C.S., Peterman, R.M., 1981. Stability of semi-arid savanna grazing systems. J. Ecol. 69, 473–498.

Weiyan, T., 1992. Shallow Water Hydrodynamics. Elsevier Science, New York.

West, N.E., 1990. Structure and function in microphytic soil crusts in wildland ecosystems of arid and semi-arid regions. Adv. Ecol. Res. 20, 179–223.

Yair, A., Shachak, M., 1987. Studies in watershed ecology of an arid area. In: Wurtele, M.O., Berkofsky, L. (Eds.), Progress in Desert Research. Rowman and Littlefield Publishers, New York, pp. 146–193.

Yizhaq, H., Gilad, E., Meron, E., 2005. Banded vegetation: biological productivity and resilience. Physica A 356 (1), 139–144.